III. RADIO ASTRONOMY[*]

Prof. A. H. Barrett	Dr. S. H. Zisk	M. A. Palfy
Prof. J. W. Graham	R. J. Allen	S. M. Rezende
Prof. M. Loewenthal	R. K. Breon	A. E. E. Rogers
Prof. R. P. Rafuse	Patricia P. Crowther	J. H. Spoor
Dr. W. B. Lenoir	A. B. Hull	D. H. Steinbrecher
Dr. D. H. Staelin	J. M. Moran, Jr.	A. Vander Vorst

A. OBSERVATIONS OF MICROWAVE EMISSION FROM ATMOSPHERIC OXYGEN

A series of four more balloon flight experiments was performed from the NCAR Balloon Base, Palestine, Texas, in July 1965.[1-3] The flight characteristics and comments on the flights are summarized in Table III-1.

Table III-1. Summary of balloon flight experiments.

Flight	Date	Duration	Float Height	Ascent	Descent	Purpose	Comments
150-P	17 July	8 hr	30 km	2 hr	2 hr	To study line shape	Data of first hour missing, otherwise successful
152-P	21 July	8 hr	39 km	2 1/2 hr	Parachute	To infer temperature profile	Successful
153-P	27 July	8 hr	39 km	2 1/2 hr	Parachute	To infer temperature profile	Successful
154-P	30 July	8 hr	30 km	2 hr	2 hr	To study line shape	Successful

The flights made to study the line shape have been previously described.[1-3]

Flights 152-P and 153-P represent the first attempt to infer the temperature profile from microwave measurements taken remotely. The only difference in the radiometer for these experiments is that the antennas are directed at 0° and 60° nadir angles (rather than 60° and 75° zenith angles as in Flights 150-P and 154-P). The resulting weighting functions are shown in Fig. III-1 under the assumptions of an altitude of 40 km and atmospheric profiles the same as those measured during Flight 55-P in July 1964. The computed brightness temperatures for the 6 channels are plotted in Fig. III-2 against height.

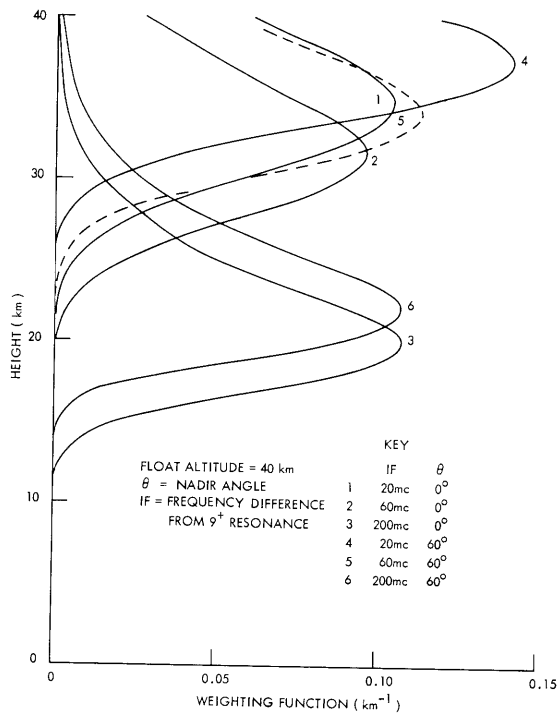The data are undergoing analysis, but preliminary indications are that the results
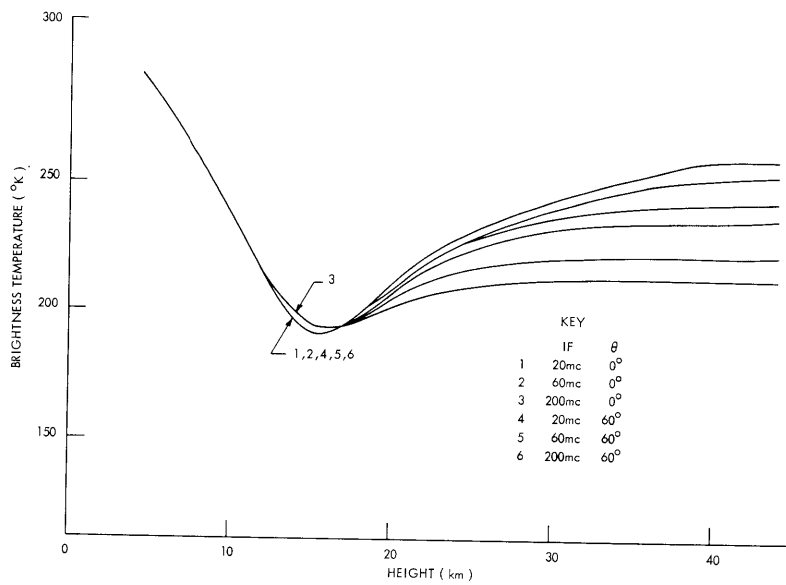
Fig. III-1. Weighting functions.

Fig. III-2. Brightness temperatures.

are very good for all flights. The PDP-1 computer is being used for partial analysis of the data for greater speed and accuracy.

W. B. Lenoir

References

1. W. B. Lenoir, Quarterly Progress Report No. 77, Research Laboratory of Electronics, M. I. T., April 15, 1965, pp. 20-23.

2. W. B. Lenoir and J. W. Kuiper, Quarterly Progress Report No. 75, Research Laboratory of Electronics, M. I. T., October 15, 1964, pp. 9-18.

3. A. H. Barrett, J. C. Blinn III, and J. W. Kuiper, Quarterly Progress Report No. 71, Research Laboratory of Electronics, M. I. T., October 15, 1963, pp. 69-76.

B. REMOTE SOUNDING OF THE UPPER ATMOSPHERE BY MICROWAVE MEASUREMENTS

1. Introduction

The Zeeman effect has been included in a rigorous analysis of the microwave spectrum of atmospheric O_2 near λ 5 mm.[1,2] On the basis of this analysis it appears possible to remotely sound the atmospheric temperature from satellite-based radiometers.

This radiometer would probably be a Dicke superheterodyne radiometer characterized by ν_o, the center frequency of the passband; BW, bandwidth; τ, post detection integration time; and T_N, effective noise temperature. The rms deviation of the receiver output expressed in temperature units would be

$$\Delta T_{rms} = \frac{2T_N}{\sqrt{BW \cdot \tau}}.$$ (1)

For a satellite in a polar orbit similar to that of a Nimbus satellite, an effective ground speed of 6 miles/sec is experienced. The desired horizontal spatial resolution will, therefore, limit the length of τ. Likewise, the desired vertical spatial resolution will limit BW.

2. Equations of Radiative Transfer

In considering the microwave emission from atmospheric oxygen the appropriate equation of propagation is the matrix equation of radiative transfer,[1,2]

$$\frac{d}{dz} \underline{\underline{T}}_B(\nu, z) + \underline{\underline{A}}(\nu, z) \underline{\underline{T}}_B(\nu, z) + \underline{\underline{T}}_B(\nu, z) \underline{\underline{A}}^{t*}(\nu, z) = 2t(z) \underline{\underline{A}}(\nu, z)$$ (2)

with

$\underline{\underline{T}}_B(v, z)$ = brightness temperature matrix

$\underline{A}(v, z)$ = attenuation matrix

$t(z)$ = kinetic temperature

z = vertical distance variable.

The formulation of Eq. 2 and the derivation of $A(v, z)$ has been reported elsewhere.[1]

The terrestrial atmosphere was approximated as a series of constant-temperature, constant-pressure layers, each 1 km thick. One hundred such layers from the ground
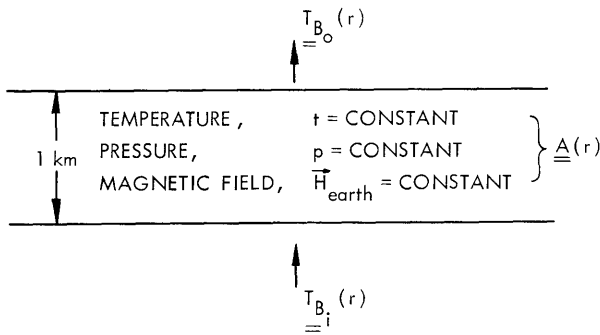

Fig. III-3.   Layer geometry.

to a height of 100 km were used. (Above 100 km there is insufficient oxygen to be of importance.) See Fig. III-3.

The solution to (2) for one such layer is

$$\underline{\underline{T}}_{B_o}(v) = e^{-\underline{\underline{A}}(v)\Delta z} \, \underline{\underline{T}}_{B_i}(v)\, e^{-\underline{\underline{A}}(v)\Delta z} + t\left[\underline{\underline{I}} - e^{-2\underline{\underline{A}}(v)\Delta z}\right]. \tag{3}$$

The ground-atmosphere interface is not of importance here because only frequencies in the center of the resonance complex are considered. For these frequencies the attenuation from the ground to 100 km is so great that emission below 10 km does not contribute to the $\underline{\underline{T}}_B(v)$ at 100 km. The $\underline{\underline{T}}_B(v)$ observable by a satellite-based radiometer is found by continual application of (3) for each of the layers between the ground and 100 km.

A somewhat different analysis, emphasizing the contribution to $\underline{\underline{T}}_B(v)$ of the individual layers, was actually used. The emission from each layer is carried through all layers above it to give its contribution to the total $\underline{\underline{T}}_B(v)$. These contributions are then summed for the $\underline{\underline{T}}_B(v)$. In this manner it is convenient to define a weighting-function matrix,

$$\underline{\underline{WF}}(z, v) = \underline{\underline{P}}(z, v)\left[\underline{\underline{I}} - e^{-2\underline{\underline{A}}(v, z)\Delta z}\right]\underline{\underline{P}}^{t*}(z, v) \tag{4}$$

with

$$\underline{\underline{P}}(z,\nu) = e^{-\underline{\underline{A}}(\nu,100)} \; e^{-\underline{\underline{A}}(\nu,99)} \cdots e^{-\underline{\underline{A}}(\nu,z+1)} \; .$$

Thus

$$\underline{\underline{T_B}}(\nu) = \sum_{z=1}^{100} \underline{\underline{WF}}(z,\nu) \, t(z). \tag{5}$$

The polarization basis for the calculations was linear polarizations along the θ and ϕ directions in the geomagnetic coordinate system. The angles are defined in Fig. III-4. The 1-1 elements of the matrices represent linear polarization with the H field in the $\pm\phi$ direction, while the 2-2 elements represent linear polarizations with the H field in
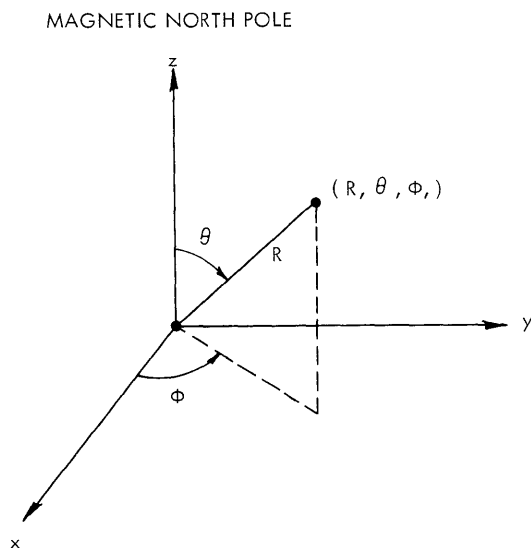
MAGNETIC NORTH POLE

Fig. III-4. Coordinate system.

the $\pm\theta$ direction.

The magnetic field model was a dipole with peak strength of 0. 62 gauss at the poles. To simplify computations, the magnitude of the field at 65 km was used for all heights (i. e., the radial dependence of the field was ignored). The total variation (peak-to-peak) of the magnitude of the field over height ranges of interest was less than 2 per cent. This is negligibly small compared with probable anomalies from a true dipole field. The direction of the dipole field is independent of height, hence no further assumption was made.

The polarization from a π component of the Zeeman split resonance is θ linear, independent of the magnetic equator. It does, however, have a $\sin^2 \theta$ amplitude dependence. The polarization from a σ component depends on latitude. For $\theta = 90°$ (magnetic equator) the polarization is ϕ linear. For $\theta = 0°$ (magnetic pole) the polarization is circular with the sense depending on which σ component is being considered. For

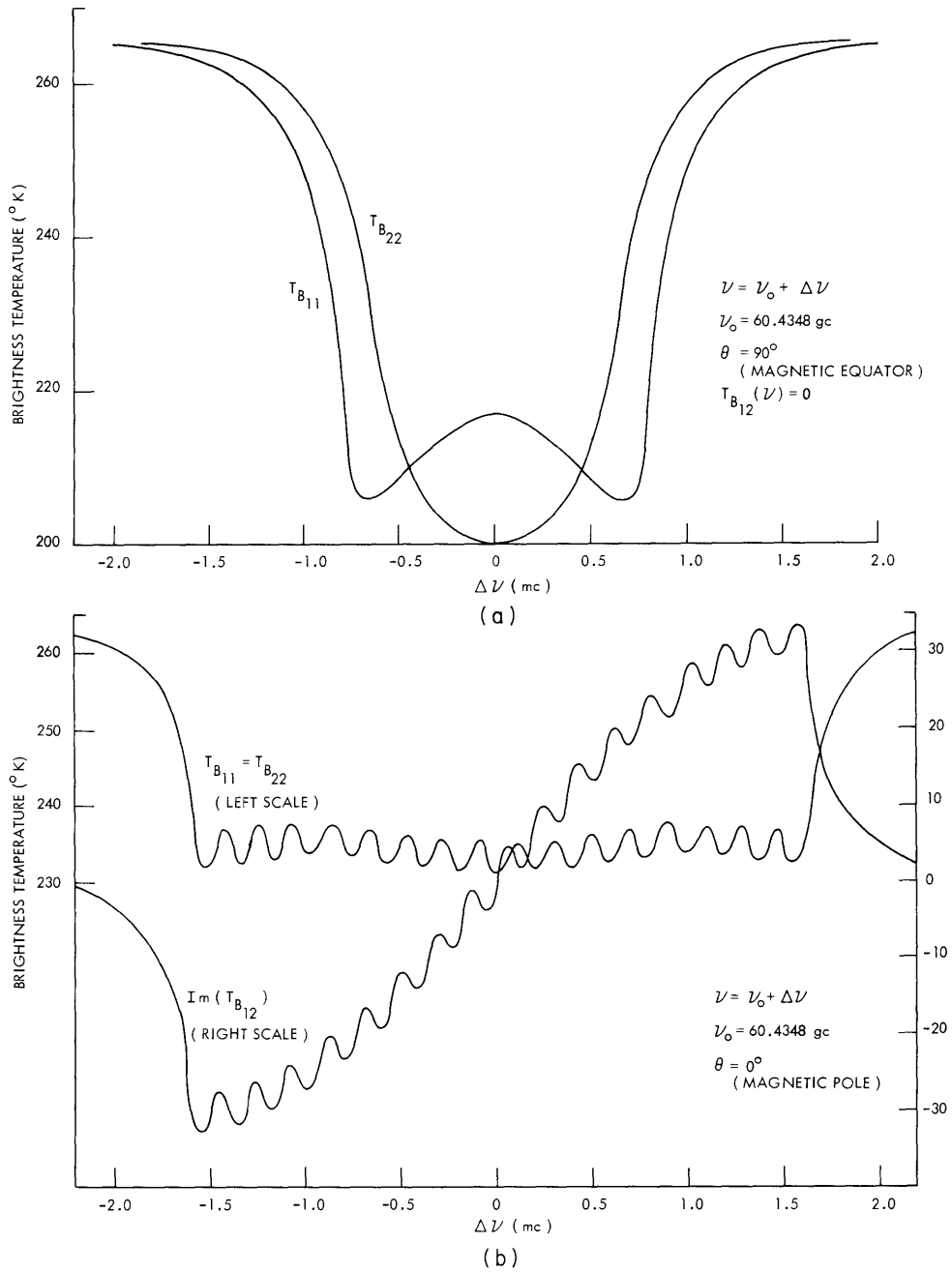Fig. III-5.   Brightness temperature spectrum, 7^+ line.   (a) Magnetic equator.
(b) Magnetic pole.

$0° \leq \theta \leq 90°$ the polarization is elliptical with the major axis in the $\pm\phi$ direction and the minor axis in the $\pm\theta$ direction (the sense again depending on the σ component).

Because of the choice of coordinate system, the real part of the off-diagonal terms of $\underline{\underline{T}}_B(\nu)$ will be zero for all latitudes. This means that there is no linear coherence between the 1-1 element and the 2-2 element, which can be seen above. The imaginary part of the off-diagonal terms can, however, be nonzero, being a measure of the circular coherence between the two main diagonal elements. The imaginary part is zero only along the magnetic equator.

3. Mesospheric Sounding

To sound the atmosphere as high as possible the most intense resonance lines should be used. The most intense lines for temperatures of 200-300°K are the 7^+ and 7^- lines. The 7^+ line has more Zeeman components than the 7^-, so the relative transparency (deeper probing) of frequencies between the Zeeman components is less. Using the 1962 U. S. Standard Atmosphere as an atmospheric model, we analyzed the 7^+ line as seen from a satellite.

$\underline{\underline{T}}_B(\nu)$ for the 7^+ line is plotted in Fig. III-5 for both the magnetic equator and the magnetic pole. An experiment with passband centered on the 7^+ resonance and with a 1.5-Mc bandwidth was found to be the best for global high-altitude sounding. The $\underline{WF}(z,\nu)$'s for this bandwidth are shown in Fig. III-6. The latitude dependence of the heights of the weighting function peaks and heights at which the weighting functions are one-half of their peak values is shown in Fig. III-7. The 7^+ line experiment is summarized in Table III-2.

Table III-2. 7^+ Experiment.

$\nu_o = 60.4348$ Gc
BW = 1.5 Mc
h_o = height of WF peaks
Δh = full width between 1/2 peak heights

	h_o	Δh
Equator, 11 polarizations	72.5 km	20 km
Equator, 22 polarizations	74 km	20 km
Pole, all polarizations	66 km	26 km

If a measurements as summarized in Table III-2 were performed with a radiometer having $T_N = 10^4$°K and $\tau = 10$ sec (60 miles on ground), the ΔT_{rms} would be 5°K. For
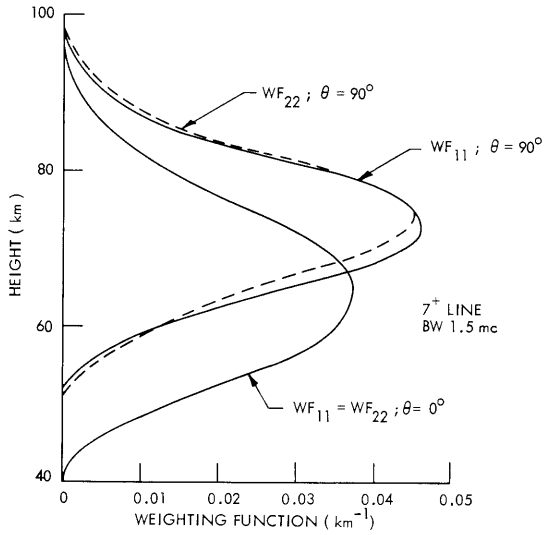
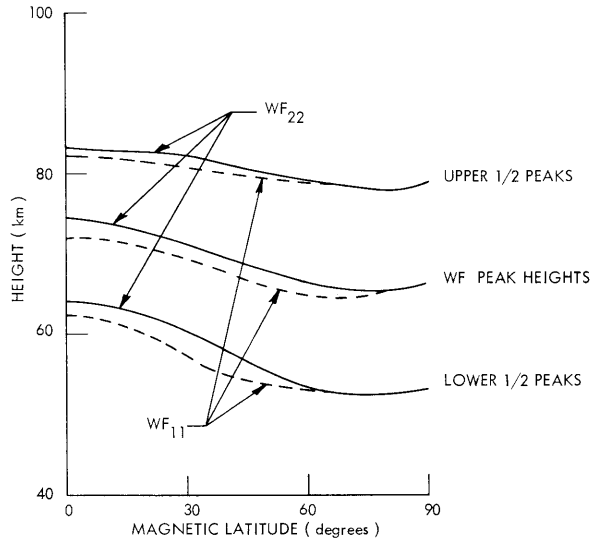Fig. III-6. Weighting functions, 7^+ line, 1.5-Mc bandwidth.

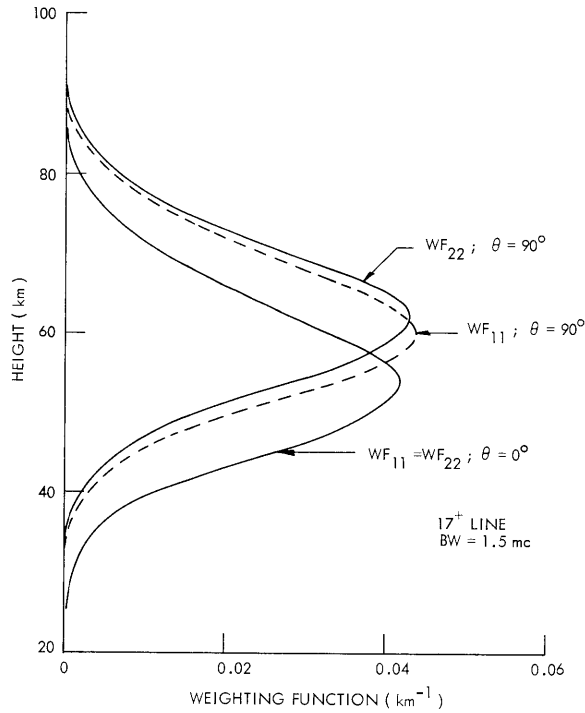
Fig. III-7. Height variation of weighting-function peaks.

Fig. III-8. Weighting functions, 17^+ line, 1.5-Mc bandwidth.

T_N = 7000°K and τ = 30 sec (180 miles), a ΔT_{rms} = 2°K results.

4. Atmospheric Soundings at 10-80 km

A weighting function peaking at 55-60 km would be the 17[+] line with a 1.5-Mc bandwidth. The WF for this experiment are shown in Fig. III-8.
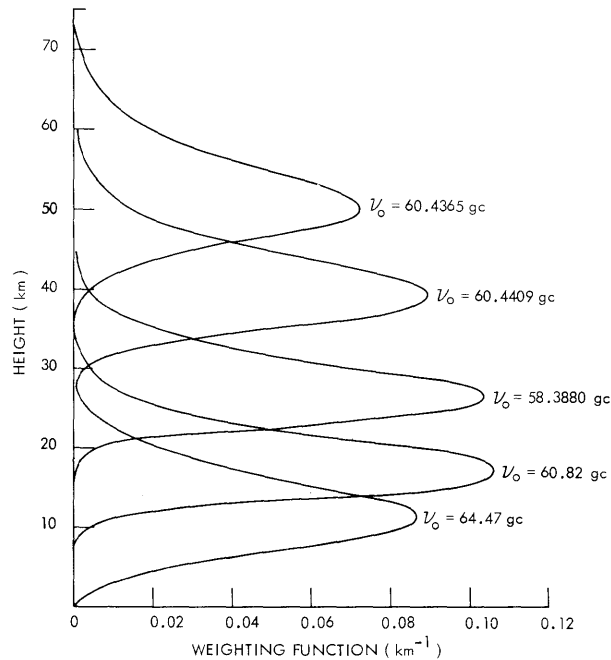

Fig. III-9. Weighting functions, 10-50 km soundings.

For WF peaking below 50 km, the Zeeman effect is not important. The pressure broadening is much larger than the Zeeman splitting and the line appears as a single, unpolarized line. Frequencies and bandwidths to cover the range 10-50 km were chosen with the bandwidth as large as possible without broadening the WF to a great extent. Table III-3 summarizes these five WF, which are plotted in Fig. III-9.

Table III-3. 10-50 km Soundings.

ν_o (gc)	BW (mc)	h_o (km)	Δh (km)
64.47	200	12	10
60.82	200	18	7
58.388	30	27	9
60.4409	2.5	40	12
60.4365	1.0	50	21

A seven-channel satellite experiment to remotely sound the atmospheric temperature could combine the seven experiments discussed above. The parameters for such an experiment are listed in Table III-4.

Table III-4. Remote sounding at 12-75 km.

$$\Delta T_1 = \Delta T_{rms} \text{ for } T_N = 10^4 {}^\circ K, \ \tau = 10 \text{ sec}$$
$$\Delta T_2 = \Delta T_{rms} \text{ for } T_N = 7000 {}^\circ K, \ \tau = 30 \text{ sec}$$

ν_o (Gc)	BW (Mc)	h_o (km)	Δh (km)	ΔT_1 (°K)	ΔT_2 (°K)
64.47	200	12	10	0.5	0.2
60.82	200	18	7	0.5	0.2
58.388	30	27	9	1.2	0.5
60.4409	2.5	40	12	4	1.5
60.4365	1.0	50	21	6	2.5
63.5685	1.5	60, equator	21	5	2
		54, pole	26		
60.4348	1.5	73, equator	20	5	2
		66, pole	26		

W. B. Lenoir

References

1. W. B. Lenoir, Ph. D. Thesis, Department of Electrical Engineering, M. I. T., June 1965.

2. W. B. Lenoir, Quarterly Progress Report No. 77, Research Laboratory of Electronics, M. I. T., April 15, 1965, pp. 24-40.

C. VARACTOR PARAMETERS

The barrier capacitance of a p-n junction is given by the well-known relationship

$$C_j = C_{min} \left[\frac{V_B + \phi}{V + \phi} \right]^\gamma , \tag{1}$$

where ϕ is the contact potential, V is the applied voltage (positive for reverse bias), V_B is the breakdown voltage, C_{min} is the junction capacitance at breakdown, and $\gamma = 0.5$

for an abrupt junction and = 0. 333 for a linearly graded junction.

The junction is not directly accessible, since the diode is mounted and packaged. The package characteristics can even be dominant at X-band. The simplest equivalent
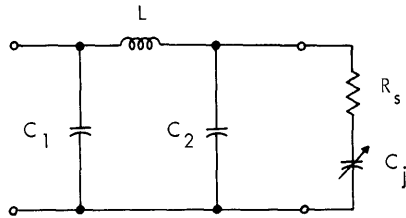

Fig. III-10.   Equivalent circuit.

circuit for the packaged diode is shown in Fig. III-10, in which the following parameters are represented:

C_j, junction capacitance

R_s, junction series resistance

L, series inductance

C_2, shunt capacitance, across the junction

C_1, exterior case capacitance.

We have studied Sylvania diodes. For these varactors two mounts are available (Fig. III-11). When examining these mounts, one suspects that the series inductance is
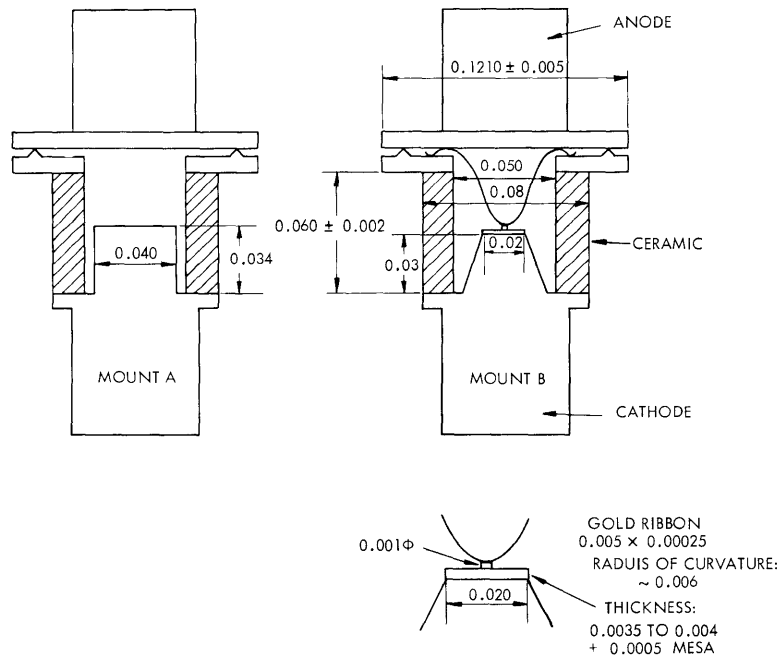

Fig. III-11.   Diode mounts.

due mostly to the inductance of the Gold ribbon that makes the contact between the mesa and the anode post. One also suspects that the total case capacitance of mount A is bigger than the total case capacitance of mount B: indeed, in mount A, the ceramic cylinder is shielded by the metallic structure, along approximately three-fifths of its height. The manufacturer tells the customer that the difference between the case capacitance of mount A and of mount B is ~0.04 pf.

The capacitance C_2 as given by the manufacturer is $C_2 \approx 0.06$ pf.

On a parallel-plate basis (with the conical structure replaced by an average horizontal plane) the total case capacitance of mount B can be calculated:

$$C_{case} = C_1 + C_2 = 0.172 \text{ pf.}$$

1. Low-Frequency Measurements

At low frequency (1 MHz) the series inductance is negligible. The only "parasitic" element is the total case capacitance.

Theoretically, only three measured values of the junction capacitance are necessary to determine the case capacitance and the exponent γ. Indeed, the total measured capacitance is

$$C = C_{case} + C_{min}\left[\frac{V_B + \phi}{V + \phi}\right]^{\gamma}. \tag{2}$$

Having measured three values C_1, C_2, and C_3, one can easily eliminate C_{min}, V_B, and C_{case}:

$$\frac{C_1 - C_2}{C_1 - C_3} = \frac{1 - \left[\dfrac{V_1 + \phi}{V_2 + \phi}\right]^{\gamma}}{1 - \left[\dfrac{V_1 + \phi}{V_3 + \phi}\right]^{\gamma}}. \tag{3}$$

There are two unknowns in this equation, ϕ and γ. The problem can be solved by iteration, until a self-consistent solution is found.

We have shown that this method leads to wrong values of γ and C_{case} because C_1, C_2, and C_3 need to be known with extremely high accuracy to get the right values of γ and C_{case}.

A computer program was written,[1] which we used to handle measurements on 16 Sylvania varactors.

The measurements are performed in a special diode holder. Its principal characteristics are the following:

1. The diode is measured between two plates to make the fringing capacitance

identical to that of the diode mounted in a reduced-height waveguide.

2. The mechanical stability is very good: an experimental repeatability of ± 0.002 pf has been measured.

There is no problem in determining by this method the case capacitance and the exponent γ of true abrupt junctions. Measurements on 6 diodes indicate that the total case capacitance of mount B and the corresponding standard deviation are $C_{case} = 0.165 \pm 0.002$ pf. The exponent was found to be 0.500 within a few per cent. Such an error is expected: it can be calculated from the errors caused by the capacitance bridge and the voltmeter (a potentiometer was used here).

The case capacitance of mount A has not been determined with such accuracy; we had either graded junctions in this mount or junctions for which the doping concentration was not uniform. In both cases the contact potential varies with the applied voltage, and our method is not so accurate. We found the following values for case capacitance: 0.190, 0.192, 0.205 pf.

2. X-band Measurements

X-band measurements were performed on a reduced-height waveguide, in use at Lincoln Laboratory, M. I. T. The transmitted power is measured at resonance and at the 3-db points. This allows one to determine[2] R_s, junction series resistance; L, series inductance (Fig. III-10); and C_2, shunt capacitance (Fig. III-11).

It has been pointed out[3] that the model of Fig. III-10 is not sufficient: a series inductance L_1 in front of it (Fig. III-12) takes into account the behavior of an inductive post in a waveguide. Indeed, the packaged diode behaves as a radial line; at resonance its input impedance is very small and the packaged diode is almost a short. The value of L_1 can be calculated: $L_1 = 0.256$ nH.
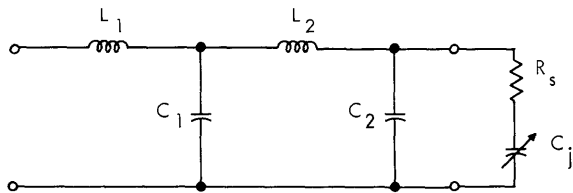

Fig. III-12. Double LC equivalent circuit.

We have verified experimentally the fact that the calculated value of the inductance L (Fig. III-10) is too large with respect to the expected value ($L_2 \approx 0.4$ nH) by an amount ≈ 0.25 nH.

The transformation of the diode impedance to the entry of the double LC circuit has been performed. It has been shown theoretically that C_1 and C_2 are almost equal at X-band (while $C_1/C_2 \approx 2$ at 1 MHz). This allows one to determine C_1 and C_2 at microwave frequencies, independently of the low-frequency value. The following results have been found at X-band for abrupt junctions in mount B:

$L_2 = 0.496 \pm 0.01$ nH

$$C_1 + C_2 = 2C_1 = 2C_2 = 0.169 \pm 0.015 \text{ pf.}$$

The total case capacitance is thus frequency-independent until X-band, since the low-frequency value was $C_{case} = 0.165 \pm 0.002$ pf.

Since C_1 and C_2 have been found to be equal (within 2%), a new model is suggested for the package: a one-dimensional transmission line. The parameters of this line have been calculated: the standard deviation is smaller on these parameters than on the lumped circuit parameters. This suggests that a transmission line is a better model than a lumped circuit. The characteristic impedance is approximately 70 Ω at X-band; it increases slowly with frequency.

A. S. Vander Vorst

References

1. D. H. Stebbins, "Data Processing Technique for Evaluating Some Parameters of Packaged Varactors," S. B. Thesis, Department of Electrical Engineering, M. I. T., June 1965.

2. D. H. Steinbrecher and W. C. Schwab, "ABC's of Varactor Measurements," Internal Memorandum, Research Laboratory of Electronics, M. I. T., 1964.

3. W. J. Getsinger, "The Packaged and Mounted Diode as a Microwave Circuit," Lincoln Laboratory preprint, July 1965.

D. SPECTRAL-LINE RADIOMETER SYSTEM AT HAYSTACK

Spectral-line radio astronomy has reached a new stage in its development with the discovery of more spectral lines in addition to the well-known 21-cm line of neutral hydrogen.[1] The 18-cm lines of OH show some extremely narrow features that require resolutions of 1 kcps, or better, to fully resolve their spectral detail.

A new spectral-line radiometer has recently been completed at the Haystack Research Facility of Lincoln Laboratory, M.I.T., to meet the demands of the field. The system uses the 120 ft parabolic dish, a parametric amplifier front end, and a 100-channel digital autocorrelator[2] in conjunction with a Univac 490 real-time computer. The parametric amplifier and feeds are usable in the frequency range 1.4-1.8 Gc/sec with system temperature of 200°K, or better. The correlator in conjunction with the computer gives spectra with total bandwidths ranging from 4 Mc to 40 kc and equivalent filter resolutions from 100 kc to 1 kc respectively.

A block diagram of the system is shown in Fig. III-13. A photograph of the control room panels is shown in Fig. III-14. The correlation and computer calculate a comparison and difference spectrum. The difference spectrum can be the difference between antenna and dummy load or the difference between antenna and sky horn. Alternatively, the ferrite switch can be locked and the difference between spectra in adjacent frequency
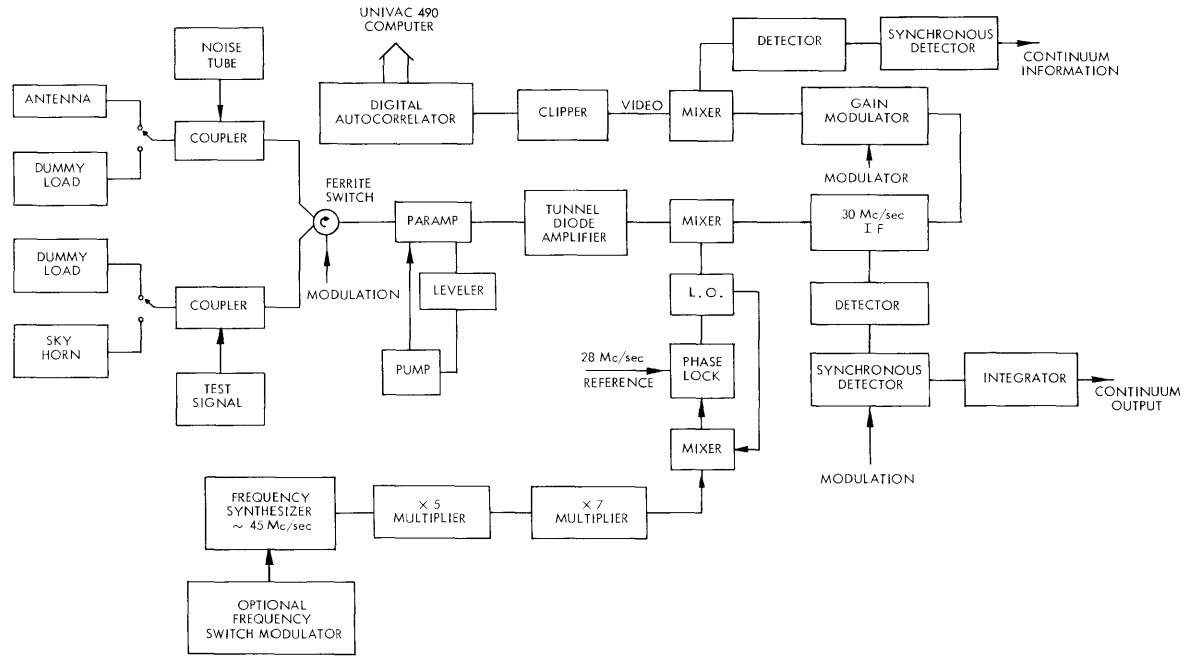
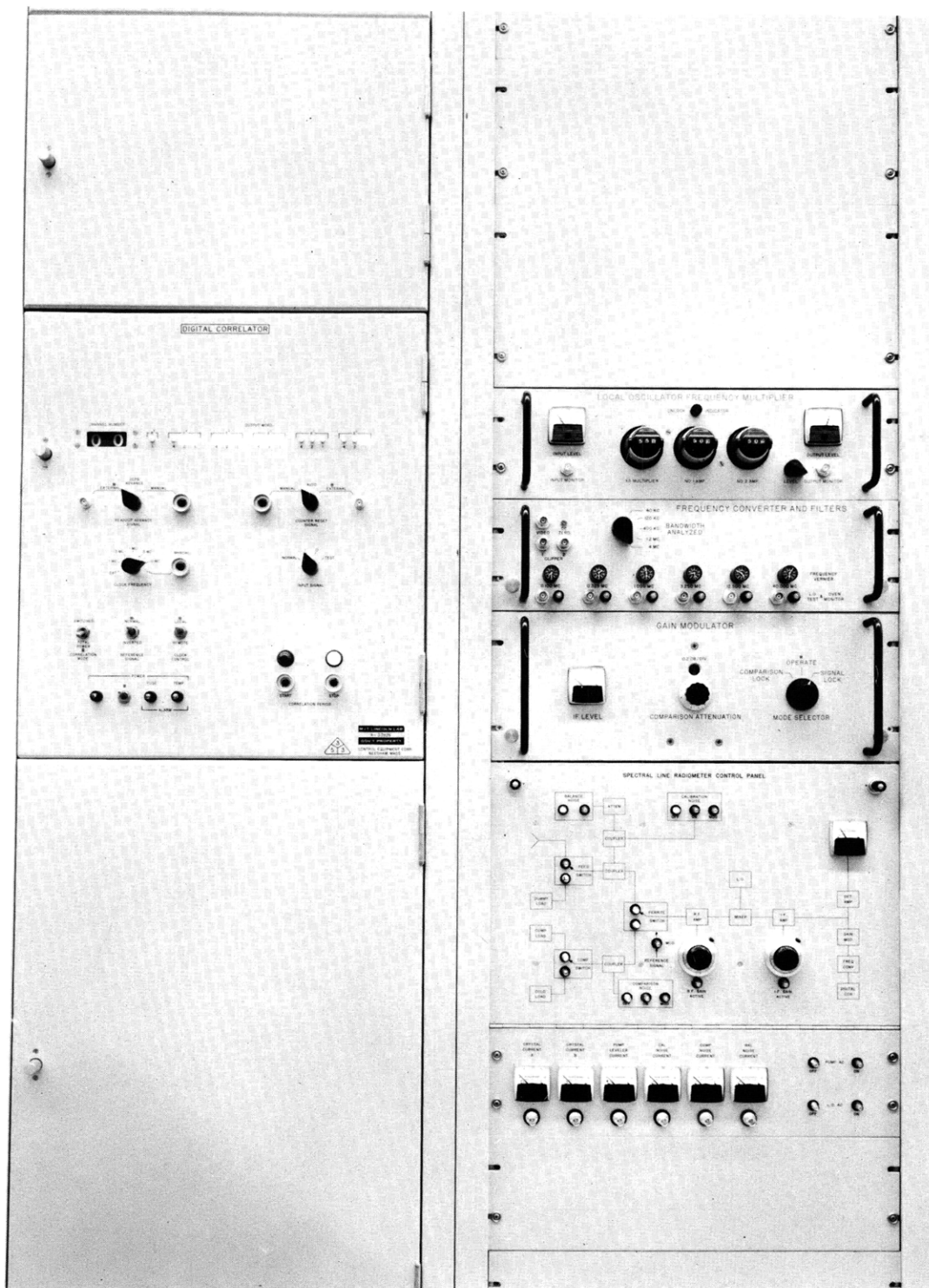Fig. III-13.   The spectral-line radiometer.

Fig. III-14.   Showing portions of the spectral-line radiometer and digital correlator.

bands taken by switching the local-oscillator frequency.

The radiometer has been used to repeat the measurement of OH absorption in the spectrum of Cassiopeia A. An integration period of 20 minutes was enough to duplicate weeks of work done at Millstone.[1]

In a recent article Weaver, Williams, Dieter, and Lum[3] reported observations of strong microwave emission lines in the HII region W3. The lines, observed at approximately 1665 Mc/sec (see Fig. III-15), exhibited complex spectral structure but could
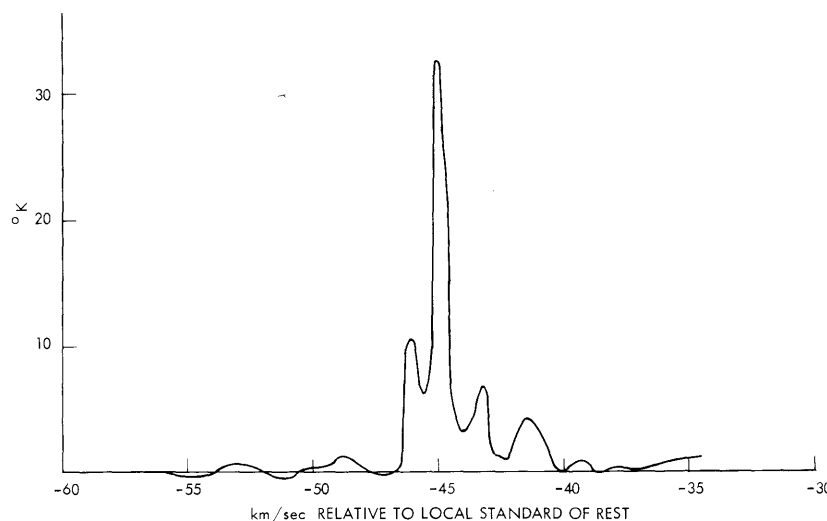

Fig. III-15. Emission spectrum in W3 at 1665 Mc.

not be detected at 1667 Mc/sec, as would be expected if the emission were attributable to OH. Weaver and his co-workers considered the lines to be unidentified and called them "mysterium." We have observed the same region and conclude that (i) emission is present not only at 1665 Mc/sec but also at 1667 Mc/sec and 1720 Mc/sec with frequency spacings as predicted from the OH spectrum; (ii) the emission at 1665 Mc/sec and 1667 Mc/sec is linearly polarized as much as 30-40 per cent; and (iii) the maximum emission is not coincident with the source W3 but displaced approximately 0.5°. These observations represent the first detection of polarized line emission in radio astronomy. Our observations are not complete but we conclude "mysterium" is really OH. The ratios of line intensities, however, are clearly anomalous. If the polarization is attributed to the Zeeman effect, the indicated magnetic fields are several orders of magnitude greater than those normally associated with the galactic interstellar medium.

A. H. Barrett, A. E. E. Rogers

References

1. A. H. Barrett, "Discovery of the Interstellar 18-cm Lines of the Hydroxyl (OH) Radical," Quarterly Progress Report No. 72, Research Laboratory of Electronics, M. I. T., January 15, 1964, pp. 28-30.

2. S. Weinreb, "A Digital Spectral Analysis Technique and its Application to Radio Astronomy," Technical Report 412, Research Laboratory of Electronics, M. I. T., August 30, 1963.

3. H. Weaver, D. R. W. Williams, N. H. Dieter, and W. T. Lum, "Observations of a Strong Unidentified Microwave Line and of Emission from the OH Molecule," Nature 208, 29-31 (1965).

E. THEORETICAL STUDIES OF RADAR ECHOES FROM THE SUN

The solar radar, near El Campo, Texas, built and originally operated by Lincoln Laboratory, M. I. T., has been operating almost continuously since April 1961. Since January 1965, the facility has been an activity of the Space Science Center, M. I. T., under the auspices of the National Aeronautics and Space Administration. The results obtained thus far have been of considerable interest, particularly since there are some very puzzling aspects in the data. In at least two areas theoretical studies should prove profitable. These have to do with explaining the great variability of the returned signal levels and the solar radar cross section deduced from them and, second, the very wide, variable, and asymmetrical Doppler spectra that have been observed.

The radar cross section computed from the data varies significantly from day to day. Most of the time the variation is from approximately 0.4 to 1.2 times the projected area of the photosphere, $\pi R_o^2 = 1.5 \times 10^8$ square meters. While this variation is difficult to account for, even harder is the large number of occasions on which the echo has been very much larger or smaller than these values. A projected area of twice πR_o^2 is not uncommon; values around $5\pi R_o^2$ have been obtained more than a dozen times, while the largest value observed was $16\pi R_o^2$. At other times, the echo has disappeared. It should be remembered that all of the solar radar observations have been made during the low part of the sunspot cycle, so that even more spectacular results might be expected as the peak period of solar activity is approached.

Characteristic of the echo spectra, which is measured at a number (~20) of range intervals, is first the large width and great variability of the spectra. Half-power widths averaging 30-40 kc/sec (the radar frequency is 38.25 Mc/sec) can vary by factors of two either way. (In fact, the spectra were much wider than anticipated so that the system had to be redesigned a number of times as the original separation of only 8 kc/sec in the frequency-shift keying of the transmitter was increased to 60 kc/sec. As a result, there are some inaccuracies in the earlier data.) The sequence of spectra shows considerable variation in both the range and range spread of the energy distribution of echoes. At the

same time, there are variations with range in the mean Doppler shift, and the peak of the Doppler spectrum. In general, but not always, the mean Doppler shift is positive and more positive for the earlier range intervals. Moreover, there is no obvious correlation between these effects and the variation of the radar cross section. Finally, the normal daily fluctuations in the echo do not correlate well with any of the other measurable effects of solar activity, K indices, and so forth. The abnormally large cross sections however, have usually occurred under disturbed conditions.

Many of these effects are difficult to explain by any model of the solar structure. Certainly, a spherically symmetric distribution of ion density hardly explains any of the facts. A somewhat more complex model, in which strong specular reflection is avoided, is obtained by allowing the reflecting surface, at least, to be rough. In addition to other troubles, such models fail in relying only on the solar rotation to produce the observed Doppler spectra; some form of motion is required. Somewhat more successful are models that introduce random scattering centers in an otherwise spherically symmetric model. Still more promising are models that introduce some systematic structure and organized mass motion. While the problem is complicated, some of the effects are so gross that something more than a casual explanation is required, and there is every assurance that concrete results should be obtainable.

Of the several models now being studied, the most promising and interesting are those involving a radial structure aligned with a radial magnetic field. Such R-rays are located in the solar corona above active areas in the photosphere and are tied in with the production of streamers and the Type II slow-drift bursts. The evidence indicates that the inhomogenieties may have longitudinal dimensions $\approx 10^5$ km. and electron densities averaging approximately 10 times those of the undisturbed solar atmosphere. The filaments may occur and re-occur at places where the magnetic structure is particularly stable. The effort involved in the study of the various propagating modes on such structures and the reflection of radio waves from them (including the effect of the solar rotation and charge motions) should prove interesting.

M. Loewenthal

References

1. J. C. James, "Radar Studies of the Sun," preprint of Chap. XI in a proposed book, Radar Astronomy, edited by J. V. Evans and Tor Hagfors (Lincoln Laboratory, M. I. T.).

2. E. R. Mustel, "On the Spatial Structure of the Solar Corona," Part I. Soviet Astronomy, A.J., Vol. 6, No. 3, pp. 333-339, 1962; Part II. Soviet Astronomy, A. J., Vol. 6, No. 4, pp. 488-496, 1963.

3. C. de Jager, "Structure and Dynamics of the Solar Atmosphere," Handbuch der Physik, Vol. 52, p. 80, 1959.

4. A. H. Maxwell and A. R. Thompson, "Spectral Observations of Radio Bursts, II. Slow-drift Bursts and Coronal Streamers," Astrophys. J. 135, 138-150 (1962).